# Dynamics and Kinetic Isotope Effects for the Intramolecular Double Proton Transfer in Oxalamidine Using Direct Semiempirical Dynamics Calculation

**Yongho Kim*,† and Hyun Jin Hwang‡**

*Contribution from the Department of Chemistry, Kyung Hee University, Yongin-City, Kyunggi-Do 449-701, Korea, and Department of Chemistry, Kyung Hee University, Seoul 130-701, Korea*

*Received December 9, 1998*

**Abstract:** We have carried out direct semiempirical dynamics calculations for the double proton transfer in oxalamidine using variational transition state theory with multidimensional semiclassical tunneling approximations. This double proton transfer occurs stepwise, with an intermediate. The energy of the intermediate relative to the reactant and the barrier height have been calculated at the G2* level of theory, which yields 20.8 and 25.1 kcal $mol^{-1}$, respectively. A quantum mechanical potential energy surface has been constructed using the AM1 Hamiltonian with specific reaction parameters (AM1-SRP) which are obtained by adjusting the standard AM1 parameters to reproduce the energetics given by the G2* level of theory. The minimum energy path has been calculated on the AM1-SRP potential energy surface, and other characteristics of the surface were calculated as needed. The hydrogenic motion is separated from the heavy atom motion along the reaction coordinate. The proton hops about 0.32 Å by tunneling, but heavy atoms do not move much while tunneling occurs. Tunneling reduces the adiabatic energy barrier by 0.67 kcal $mol^{-1}$. Rate constants and kinetic isotope effects (KIEs) have been determined experimentally in methylcyclohexane and acetonitrile solutions for a bicyclic oxalamidine. The calculated KIEs agree very well with the experimental values. The calculated activation energy is about 35% higher than the measured value. The equilibrium isotope effects and the quasiclassical secondary KIEs reveal that proton transfer and the change in the force constants are asynchronous. Although the geometric parameters for the transition state (TS) are closer to those for the intermediate than those for the reactant (TS is late geometrically), the force constants are more similar to those of the reactant (TS is early in terms of force constants). The change in force constants is a nonlinear function of the geometric parameters, and depends on the position.

## Introduction

Proton transfer is one of the simplest and the most fundamental reactions in chemistry. It is important in oxidation−reduction reactions and in many other chemical and biological reactions.[1,2] Multiproton transfer, in which more than one proton is transferred, either synchronously or asynchronously, is very important in proton relay systems in enzymes, proton transfers in DNA base pairs, and prototropic tautomerisms in many hydrogen-bonded complexes. Because of the light mass of the transferred atom, the importance of tunneling in proton transfer reactions has been discussed for many years.[3] Recently many theoretical studies with ab initio quantum chemical methods at various levels have been carried out to predict the structures of hydrogen-bonded dimers and the potential energy surfaces (PESs) for various double proton transfer processes.[4−13] It has been shown that the height and shape of the PES depend strongly on the theoretical level of calculation, the size of the basis set, and the inclusion of correlation energy.[4−6,14,15] Since most of the earlier studies have focused on the geometrical change on dimerization and the energetic stabilization due to the hydrogen bonds in the dimer, the dynamic features of the double proton transfer, such as tunneling and the effect of isotopic substitution, are not yet very well understood. To study the dynamics of such systems, detailed information about the potential energy surface near the TS and the critical configuration is needed. It was not easy to obtain such information until recently.

†Yongin-City, Kyunggi-Do, Korea.
‡ Seoul, Korea.

(1) Bender, M. L. *Mechanisms of Homogeneous Catalysis from Protons to Proteins*; John Wiley & Sons: New York, 1971.
(2) Melander, L.; Saunders, W. H. J. *Reaction Rates of Isotopic Molecules*; John Wiley and Sons: New York, 1980.
(3) Bell, R. P. *The Tunnel Effect in Chemistry*; Chapman and Hall: New York, 1980.
(4) Florian, J.; Hrouda, V.; Hobza, P. *J. Am. Chem. Soc.* **1994**, *116*, 1457.
(5) Hrouda, V.; Florian, J.; Hobza, P. *J. Phys. Chem.* **1993**, *97*, 1542.
(6) Hrouda, V.; Florian, J.; Polesek, M.; Hobza, P. *J. Phys. Chem.* **1994**, *98*, 4742.
(7) Tachibana, A.; Koizumi, M.; Tanaka, E.; Yamabe, T.; Fukui, K. *J. Mol. Struct.* **1989**, *200*, 207.
(8) Tachibana, A.; Ishizuka, N.; Yamabe, T. *J. Mol. Struct.* **1991**, *228*, 259.
(9) Topaler, M. S.; Mamaev, V. M.; Gluz, Y. B.; Minkin, V. I.; Simkin, B. Y. *J. Mol. Struct.* **1991**, *236*, 393.
(10) Agranat, I.; Riggs, N. V.; Radom, L. *J. Chem. Soc., Chem. Commun.* **1991**, *1991*, 80.
(11) Zielinski, T. J.; Poirier, R. A. *J. Comput. Chem.* **1984**, *5*, 466.
(12) Svensson, P.; Bergman, N.-Å.; Ahlberg, P. *J. Chem. Soc., Chem. Commun.* **1990**, *1990*, 862.
(13) Svensson, P.; Bergman, N.-Å.; Ahlberg, P. *J. Chem. Soc., Chem. Commun.* **1990**, *1990*, 82.
(14) Scheiner, S. In *Reviews in Computational Chemistry*; Lipkowitz, K. B., Boyd, D. B., Eds.; VCH: New York, 1991; Vol. 2, p 165.
(15) Scheiner, S. In *Proton Transfer in Hydrogen Bonded Systems*; Bountis, T., Ed.; Plenum: New York, 1992; p 29.

10.1021/ja984242z CCC: $18.00 
Published on Web 04/29/1999

Formic acid dimer (FAD) is one of the simplest examples of a multiple proton transfer system in which the constituents are held together by two hydrogen bonds, so it can be used as a model for many chemically and biologically important multiple proton transfers. It is one of most extensively studied systems both theoretically and experimentally.[16−21] Recently, a direct semiempirical dynamics study for FAD showed that tunneling is very important and that the most probable tunneling path is very different from the minimum energy path (MEP).[20] There have also been several studies of double proton transfer in monohydrated formamidine,[22−26] since amidine molecules have many biological and pharmaceutical functions. Tunneling is also very important in this reaction, and the most probable tunneling path is again very different from the MEP, although the reaction path curvature near the TS is small.[22] Recently Limbach et al. have studied intramolecular double proton transfer in the prototropic tautomerisms of porphyrins and azophenine using the dynamic NMR technique,[27−32] and found that the double proton transfer has a stepwise pathway. Stepwise pathways have also been proposed theoretically for these reactions.[33−38] Limbach and co-workers have studied the double proton transfer in oxalamidine, and obtained kinetic HH/HD/DD isotope effects as well as solvent effects, which indicated a stepwise pathway with a zwitterionic intermediate.[39−41] The KIE values for HH/DD, HH/HD, and HD/DD were 4.8, 3.1, and 1.5, respectively, at 298 K in methylcyclohexane. These values were increased in a polar solvent. They have also performed semiempirical quantum mechanical calculations for various oxalamidine systems and concluded that the heavy atom motions would be very important in the proton tautomerization.[42]

Besides the biological importance of these reactions, it is interesting to compare the dynamics and tunneling effects in stepwise intramolecular double proton transfers with concerted intermolecular double proton transfers. However, there have been few theoretical studies of the dynamics of the oxalamidine tautomerism. No calculations of rate constants including tunneling effects have been reported up to date. Therefore, we have carried out direct dynamics calculations for the intramolecular double proton transfer by variational transition state theory, including tunneling contributions by multidimensional semiclassical approximations. A semiempirical molecular orbital method at the NDDO level, such as the AM1 or PM3 method, was used with specific reaction parameters (SRP) to calculate the minimum energy path and the potential energy along it.[43,44] The AM1 method produced an unreasonably large barrier height for the double proton transfer, so the standard AM1 parameters should be modified for this specific situation. The optimum AM1 parameters would be based on accurate energetics at the stationary points. To obtain information about the energetics of double proton transfer that is accurate enough to calibrate the AM1 parameters, the G2* level of calculation was used. In G2* theory, polarization functions on hydrogen are added to the standard G2 level basis sets.[45−47] The standard NDDO parameters were adjusted to reproduce the reaction energy and the theoretical potential energy barrier height determined by the G2* level calculations. The modified parameters, called AM1-SRP, were used for the direct dynamic calculations. The calculated reaction coordinate, tunneling effect, rate constants, and primary and secondary KIEs for the intramolecular double proton transfer in oxalamidine are reported in this paper. The asynchrony of proton transfer with respect to the change in force constants is also discussed.

## Theory

Rate constants were calculated by canonical variational transition-state (CVT) theory.[48−54] The TS was located at the position on the minimum energy path (MEP) where the calculated rate is a minimum. The Born−Oppenheimer potential on the MEP is called $V_{MEP}(s)$, where $s$ is the reaction coordinate parameter, and the canonical variational transition state theory rate constant is given by[52,55]

$$k^{CVT}(T) = \min_{s} k^{GT}(T,s) = \sigma \frac{k_B T}{h} \frac{Q^{GT}(T,s_*^{CVT})}{Q^R} \exp[-V_{MEP}(s_*^{CVT})] \qquad (1)$$

(16) Chang, Y.-T.; Yamaguchi, Y.; Miller, W. H.; Schefer, H. F., III. *J. Am. Chem. Soc.* **1987**, *109*, 7245.
(17) Shida, N.; Barbara, P. F.; Almlof, J. *J. Chem. Phys.* **1991**, *94*, 3633.
(18) Bertie, J. E.; Michaelian, K. H. *J. Chem. Phys.* **1982**, *76*, 886.
(19) Bertie, J. E.; Michaelian, K. H.; Eysel, H. H. *J. Chem. Phys.* **1986**, *85*, 4779.
(20) Kim, Y. *J. Am. Chem. Soc.* **1996**, *118*, 1522.
(21) Lim, J.-H.; Lee, E. K.; Kim, Y. *J. Phys. Chem.* **1997**, *101*, 2233.
(22) Kim, Y. *J. Phys. Chem. A* **1998**, *102*, 3025.
(23) Nguyen, K. A.; Gordon, M. S.; Truhlar, D. G. *J. Am. Chem. Soc.* **1991**, *113*, 1596.
(24) Zhang, Q.; Bell, R.; Truong, T. N. *J. Phys. Chem.* **1995**, *99*, 592.
(25) Yamabe, T.; Yamashita, K.; Kaminoyama, M.; Koizumi, M.; Tachibana, A.; Fukui, K. *J. Phys. Chem.* **1984**, *88*, 1459.
(26) Bell, R. L.; Truong, T. N. *J. Chem. Phys.* **1994**, *101*, 10442.
(27) Schlabach, M.; Rumpel, H.; Limbach, H.-H. *Angew. Chem.* **1989**, *101*, 84.
(28) Schlabach, M.; Rumpel, H.; Limbach, H.-H. *Angew. Chem., Int. Ed. Engl.* **1989**, *28*, 76.
(29) Schlabach, M.; Scherer, G.; Limbach, H.-H. *J. Am. Chem. Soc.* **1991**, *113*, 3550.
(30) Schlabach, M.; Limbach, H.-H.; Shu, A.; Bunnenberg, E.; Tolf, B.; Djerassi, C. *J. Am. Chem. Soc.* **1993**, *115*, 4554.
(31) Rumpel, H.; Limbach, H.-H. *J. Am. Chem. Soc.* **1989**, *111*, 5429.
(32) Rumpel, H.; Limbach, H.-H.; Zachmann, G. *J. Phys. Chem.* **1989**, *93*, 1812.
(33) Holloway, M. K.; Reynolds, C. H.; Merz, K. M. *J. Am. Chem. Soc.* **1989**, *111*, 3466.
(34) Dewar, M. J. S.; Merz, K. M. *J. Mol. Struct.: THEOCHEM* **1985**, *124*, 183.
(35) Merz, K. M.; Reynolds, C. H. *J. Chem. Soc., Chem. Commun.* **1988**, 90.
(36) Sarai, A. *J. Chem. Phys.* **1982**, *76*, 5554.
(37) Sarai, A. *J. Chem. Phys.* **1984**, *80*, 5431.
(38) Smedarchina, Z.; Siebrand, W.; Zerbetto, F. *Chem. Phys.* **1989**, *136*, 285.
(39) Otting, G.; Rumpel, H.; Meschede, L.; Scherer, G.; Limbach, H. H. *Ber. Bunsen-Ges. Phys. Chem.* **1986**, *90*, 1122.
(40) Scherer, G.; Limbach, H.-H. *J. Am. Chem. Soc.* **1994**, *116*, 1230.
(41) Scherer, G.; Limbach, H.-H. *J. Am. Chem. Soc.* **1989**, *111*, 5946.
(42) Scherer, G.; Limbach, H. H. *Croat. Chem. Acta* **1994**, *67*, 431.
(43) Liu, Y.-P.; Lynch, G. C.; Truong, T. N.; Lu, D.-H.; Truhlar, D. G.; Garrett, B. C. *J. Am. Chem. Soc.* **1993**, *115*, 2408.
(44) Liu, Y.-P.; Lu, D.-h.; Gonzalez-Lafont, A.; Truhlar, D. G.; Garrett, B. C. *J. Am. Chem. Soc.* **1993**, *115*, 7806.
(45) Pople, J. A.; Head-Gordon, M.; Fox, D. J.; Raghavachari, K.; Curtiss, L. A. *J. Chem. Phys.* **1989**, *90*, 5652.
(46) Curtiss, L. A.; Jones, C.; Trucks, G. W.; Raghavachari, K.; Pople, J. A. *J. Chem. Phys.* **1990**, *93*, 2537.
(47) Curtiss, L. A.; Raghavachari, K.; Trucks, G. W.; Pople, J. A. *J. Chem. Phys.* **1991**, *94*, 7221.
(48) Tucker, S. C.; Truhlar, D. G. In *New Theoretical Concepts for Understanding Organic Reactions*; Bertran, J., Csizmadia, I. G., Eds.; Kluwer: Dordrecht, The Netherlands, 1989; pp 291−346.
(49) Truong, T. N. *J. Chem. Phys.* **1994**, *11*, 8014.
(50) Truhlar, D. G.; Garrett, B. C. *J. Chem. Phys.* **1979**, *70*, 1593.
(51) Truhlar, D. G.; Garrett, B. C. *J. Chim. Phys. Phys.-Chim. Biol.* **1987**, *84*, 365.
(52) Truhlar, D. G.; Isaacson, A. D.; Garrett, B. C. In *Theory of Chemical Reaction Dynamics*; Baer, M., Ed.; CRC Press: Boca Raton, FL, 1985; Vol. 4, p 65.
(53) Truhlar, D. G.; Garrett, B. C. *Annu. Rev. Phys. Chem.* **1984**, *35*, 159.
(54) Truhlar, D. G.; Isaacson, A. D.; Skodje, R. T.; Garrett, B. C. *J. Phys. Chem.* **1982**, *86*, 2252.

The superscript GT denotes generalized transition-state theory, $k_B$ is the Boltzman constant, $h$ is Planck's constant; $s_*^{CVT}$ is the value of $s$ at which $k^{GT}$ is minimized, that is, the location of the canonical variational transition state, $\sigma$ is a symmetry factor, and $Q^{GT}$ and $Q^R$ are partition functions for the generalized transition state and reactants, respectively.

To include the tunneling effect, the calculated rate constant, $k^{CVT}(T)$, is multiplied by a transmission coefficient, $\kappa^{CVT/G}$.

$$k^{CVT/G}(T) = \kappa^{CVT/G}(T)\, k^{CVT}(T) \tag{2}$$

The transmission coefficient is defined as the ratio of the thermally averaged quantal ground-state transmission probability, $P^G(E)$, to the thermally averaged classical transmission probability for the effective potential along the reaction coordinate that is implied by CVT theory, $P_C^{CVT/G}(E)$:

$$\chi^{CVT/G}(T) = \frac{\int_0^\infty P^G(E) e^{-E/k_B T}\, dE}{\int_0^\infty P_C^{CVT/G}(E) e^{-E/k_B T}\, dE} \tag{3}$$

Since the value of $P_C^{CVT/G}(E)$ is unity above the threshold energy of the CVT calculation and is zero below, this expression reduces to

$$\kappa^{CVT/G}(T) = \frac{1}{k_B T} e^{V_a^G(s_*^{CVT})/k_B T} \int_0^\infty P^G(E) e^{-E/k_B T}\, dE \tag{4a}$$

$$= \frac{1}{k_B T} \kappa^{CVT/CAG} \int_0^\infty [P^G(E) e^{V^{AG}/k_B T}] e^{-E/k_B T}\, dE \tag{4b}$$

where

$$\kappa^{CVT/CAG} = e^{[V_a^G(s_*^{CVT}) - V^{AG}]/k_B T} \tag{4c}$$

and where $V_a^G(s_*^{CVT})$ is the ground-state adiabatic barrier evaluated at the canonical variational transition state and $V^{AG}$ is defined by

$$V^{AG} = \max_s V_a^G(s) \tag{4d}$$

Several semiclassical tunneling approximations were used to calculate $P^G(E)$. When the reaction path curvature is negligible so that the tunneling path coincides with the MEP, the minimum energy path semiclassical adiabatic ground-state (MEPSAG) method is appropriate.[56] If the reaction path is curved but the curvature is small, tunneling is assumed to occur on a path defined by the classical turning points on the concave side of the MEP. This is an example of corner-cutting tunneling. For a polyatomic system with small reaction-path curvature, the centrifugal-dominant small-curvature semiclassical adiabatic ground-state (CD-SCSAG) tunneling approximation is appropriate.[43] When the reaction path curvature is large, which is typical for a bimolecular light-atom transfer between two heavy atoms, the large-curvature ground-state approximation, version 3 (LCG3), is appropriate.[52,55,57]

The microcanonical optimized multidimensional tunneling ($\mu$OMT) approximation estimates the optimal transmission probability as the larger of the transmission probabilities evaluated by the CD-SCSAG and LCG3 methods at a given energy.[44] The MEPSAG, CD-SCSAG, and LCG3 methods are called "zero-curvature tunneling" (ZCT), "small-curvature tunneling" (SCT), and "large-curvature tunneling" (LCT) approximations, respectively. The detailed mathematical derivations and computational formulas have been discussed and reviewed elsewhere.[52,55−57]

## Computational Method

All electronic structure calculations were done using the GAUSSIAN 94 quantum mechanical package.[58] Geometries for oxalamidine, the high-energy intermediate, and the TS were optimized at the Hartree−Fock (HF) level of theory and the second-order Møller−Plesset (MP2) level of theory using various basis sets. Density functional theory calculations were also performed. Becke's gradient-corrected exchange[59] and three-parameter gradient-corrected exchange functionals[60] with Lee−Yang−Parr[61] gradient-corrected correlation (B-LYP and B3-LYP) were employed. Energies at the stationary points have also been calculated at the G2* level of theory. In the standard G2 method,[45−47] MP2(full)/6-31G(d) is used for the optimization of the geometry and energy. In this study, polarization functions on hydrogen were added because hydrogen bonding is important, so the G2 type of energies in this study will be called G2* energies. The detailed descriptions of this method have been reported previously.[20]

Direct dynamics calculations were performed using the MORATE program.[62] Frequencies were calculated as needed from MOPAC which was implemented in the MORATE program. The Page−McIver method[63] was employed to calculate the minimum energy path (MEP). The MEP is scaled to a reduced mass $\mu$ of 1 amu. To take into account the tunneling effect, the CD-SCSAG (SCT), LCG3 (LCT), and $\mu$OMT methods were used. In the LCG3 method, tunneling amplitudes are calculated from the vibrational ground state of the reactant to all accessible vibrationally excited states of the product. Rates were calculated by canonical variational transition-state theory using eqs 1−4 above.

## Results and Discussion

In the reaction coordinate for the double proton transfer in oxalamidine there is no transition state for a synchronous pathway. Instead, there is a stable intermediate with $C_{2v}$ symmetry, which is generated by a single proton transfer. This result suggests that two protons in oxalamidine are transferred asynchronously via a stepwise mechanism as depicted in Figure 1. The energies for oxalamidine (R), the transition state (TS), and the intermediate (I) have been calculated using many different levels of quantum mechanical electronic structure theory. The difference in energy between R and I ($\Delta E$) and the barrier heights ($\Delta E^*$) are listed in Table 1. They depend very

(55) Garrett, B. C.; Joseph, T.; Truong, T. N.; Truhlar, D. G. *Chem. Phys.* **1989**, *136*, 271.
(56) Garrett, B. C.; Truhlar, D. G.; Grev, R. S.; Magnuson, A. W. *J. Phys. Chem.* **1980**, *84*, 1730.
(57) Lu, D.-h.; Truong, T. N.; Melissas, V. S.; Lynch, G. C.; Liu, Y.-P.; Garrett, B. C.; Steckler, R.; Isaacson, A. D.; Rai, S. N.; Hancock, G. C.; Lauderdale, J. G.; Joseph, T.; Truhlar, D. G. *Comput. Phys. Commun.* **1992**, *71*, 235.
(58) Frisch, M. J.; Trucks, G. W.; Schlegel, H. B.; Gill, P. M. W.; Johnson, B. G.; Robb, M. A.; Cheeseman, J. R.; Keith, T. A.; Petersson, G. A.; Montgomery, J. A.; Raghavachari, K.; Al-Laham, M. A.; Zakrzewski, V. G.; Ortiz, J. V.; Foresman, J. B.; Cioslowski, J.; Stefanov, B. B.; Nanayakkara, A.; Challacombe, M.; Peng, C. Y.; Ayala, P. Y.; Chen, W.; Wong, M. W.; Andres, J. L.; Replogle, E. S.; Gomperts, R.; Martin, R. L.; Fox, D. J.; Binkley, J. S.; Defrees, D. J.; Baker, J.; Stewart, J. P.; Head-Gordon, M.; Gonzalez, C.; Pople, J. A. *Gaussian 94*; Gaussian, Inc.: Pittsburgh, 1995.
(59) Becke, A. D. *Phys. Rev. A* **1988**, *38*, 3098.
(60) Becke, A. D. *J. Chem. Phys.* **1993**, *98*, 5648.
(61) Lee, C.; Yang, W.; Parr, R. G. *Phys. Rev. B* **1988**, 786.
(62) Chuang, Y.-Y.; Hu, W.-P.; Lynch, G. C.; Liu, Y.-P.; Truhlar, D. G. MORATE-version 7.2, University of Minnesota, Minneapolis, 1997, based on POLYRATE-version 7.2 by Steckler, R.; Chuang, Y.-Y.; Coitino, E. L.; Fast, P. L.; Corchado, J. C.; Hu, W.-P.; Liu, Y.-P.; Lynch, G. C.; Nguyen, K. A.; Jackels, C. F.; Gu, M. Z.; Rossi, I.; Clayton, S.; Melissas, V. S.; Garrett, B. C.; Isaacson, A. D.; Truhlar, D. G., University of Minnesota, Minneapolis, 1997, and MOPAC-version 5.05mn by Stewart, J. J.; Rossi, I.; Hu, W.-P.; Lynch, G. C.; Liu, Y.-P.; Truhlar, D. G., University of Minnesota, Minneapolis, 1995.
(63) Page, M.; McIver, J. W. *J. Chem. Phys.* **1988**, *88*, 922.

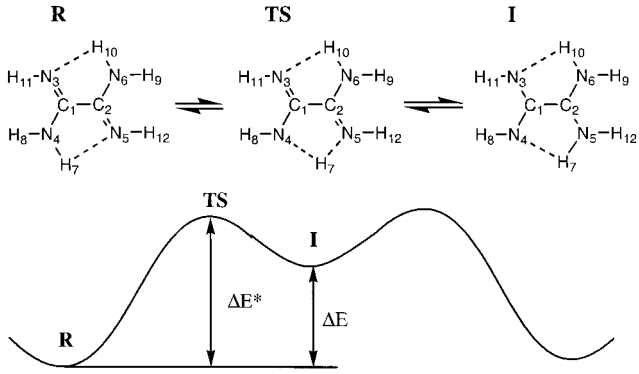


**Figure 1.** Schematic potential energy diagram for the stepwise double proton transfer in oxalamidine.

**Table 1.** Barrier Heights and Relative Energies of the Intermediate with Respect to the Reactant at Various Levels of Theory

| computational level | $\Delta E$ (kcal/mol) | $\Delta E^*$ (kcal/mol) | freq ($cm^{-1}$)[a] |
|---|---|---|---|
| AM1 | 35.72 | 52.07 | 1810i |
| HF/6-31G** | 24.19 | 32.58 | 1665i |
| HF/6-31+G** | 22.85 | 32.62 | 1733i |
| B3LYP/6-31G** | 19.96 | 22.28 | 1034i |
| B3LYP/6-31+G** | 19.08 | 22.52 | 1162i |
| B3LYP/6-31+G** (SCRF)[b] | 14.34 | 19.92 | 1395i |
| B3LYP/6-311G** | 19.73 | 22.65 | 1144i |
| BLYP/6-31G** | 18.85 | 20.56 | 904i |
| BLYP/6-31+G** | 18.03 | 20.81 | 1046i |
| BLYP/6-311G** | 18.62 | 20.94 | 1035i |
| MP2(full)/6-31G** | 22.26 | 24.93 | 1080i |
| E(G2*)[c] | 20.10 | 22.09 | |
| E(G2*)-ZPE | 20.77 | 25.10 | |
| AM1-SRP | 20.72 | 25.05 | 1284i |

[a] Reaction coordinate frequency [b] Dielectric constant $\epsilon = 40.0$. [c] The zero-point energies were weighted by 0.95.

much on the levels of quantum mechanical calculations and the inclusion of electron correlation.[13,20] The $\Delta E$ values at the HF/6-31+G(d,p) and B3LYP/6-31+G(d,p) levels are 22.85 and 19.08 kcal $mol^{-1}$, respectively. The $\Delta E^*$ values at the HF/6-31+G(d,p), B3LYP/6-31+G(d,p), and MP2(full)/6-31G(d,p) levels are 32.62, 22.52, and 24.93 kcal $mol^{-1}$, respectively. The $\Delta E$ and $\Delta E^*$ values at the BLYP level are slightly lower than those at the B3LYP and MP2 levels. The reaction coordinate frequencies were also calculated. The frequencies at the AM1 and HF levels are all larger, but those at the B3LYP and BLYP levels are similar to the MP2 value. The $\Delta E$ values are 20.10 and 20.77 kcal $mol^{-1}$ and the barrier heights 22.09 and 25.05 kcal $mol^{-1}$ from the G2* level of calculations with and without zero-point energy correction, respectively. The $\Delta E^*$ value at the MP2(full)/6-31G(d,p) level agrees very well with the G2* value, while the $\Delta E$ value is slightly larger. The solvent effect was calculated at the B3LYP/6-31+G(d,p) level using the Onsager dielectric continuum model.[64] The $\Delta E$ and $\Delta E^*$ values were reduced, but the reaction coordinate frequency and the energy difference between I and TS were increased by the solvent effect.

The geometric parameters for R, I, and the TS, optimized at the MP2(full)/6-31G(d,p) and NDDO levels using standard AM1 parameters are listed in Table 2. The optimized structure for oxalamidine has $C_2$ symmetry with an axis perpendicular to the $C_1-C_2$ bond. The intramolecular H-bond distance between $N_5$ and $H_7$ in oxalamidine, $R(5,7)$, is 2.17 Å at the MP2 level, but this distance from the AM1 method is 2.65 Å, which is 0.49 Å

(64) Onsager, L. *J. Am. Chem. Soc.* **1936**, *58*, 1486.

**Table 2.** Geometric Parameters for Oxalamidine, the Intermediate, and the Transition State, Optimized with the MP2(full)/6-31G(d,p), AM1, and AM1-SRP Methods[a]

| | MP2 | AM1 | AM1-SRP |
|---|---|---|---|
| | Oxalamidine | | |
| $R(1,2)$ | 1.506 | 1.545 | 1.519 |
| $R(2,5)$ | 1.291 | 1.296 | 1.293 |
| $R(1,4)$ | 1.366 | 1.401 | 1.377 |
| $R(4,7)$ | 1.010 | 0.995 | 0.997 |
| $R(5,7)$ | 2.165 | 2.652 | 2.296 |
| $\theta(1,2,5)$ | 117.3 | 116.3 | 119.7 |
| $\theta(4,1,2)$ | 113.3 | 114.2 | 114.9 |
| $\theta(1,4,7)$ | 113.8 | 115.9 | 115.7 |
| $\theta(4,7,5)$ | 107.9 | 98.3 | 106.2 |
| $\theta(2,5,7)$ | 85.6 | 71.4 | 83.1 |
| $\omega(5,2,1,3)$ | −166.8 | −122.4 | −172.4 |
| $\omega(6,2,1,4)$ | −163.5 | −116.2 | −171.9 |
| $\omega(5,2,1,4)$ | 14.8 | 60.7 | 7.8 |
| $\omega(2,1,4,7)$ | −16.0 | −20.1 | −2.8 |
| | Intermediate | | |
| $R(1,2)$ | 1.535 | 1.574 | 1.523 |
| $R(1,4)$ | 1.295 | 1.328 | 1.322 |
| $R(2,5)$ | 1.303 | 1.350 | 1.346 |
| $R(5,7)$ | 1.005 | 1.000 | 1.025 |
| $R(4,7)$ | 2.078 | 2.559 | 2.104 |
| $\theta(4,1,2)$ | 110.1 | 109.7 | 112.3 |
| $\theta(1,2,5)$ | 117.6 | 118.2 | 119.0 |
| $\theta(2,5,7)$ | 113.3 | 117.4 | 108.3 |
| $\theta(4,7,5)$ | 108.9 | 96.5 | 113.0 |
| $\theta(1,4,7)$ | 90.1 | 77.1 | 87.4 |
| $\omega(5,2,1,3)$ | 180.0 | −130.2 | 180.0 |
| $\omega(6,2,1,4)$ | 180.0 | −130.2 | 180.0 |
| $\omega(5,2,1,4)$ | 0.0 | 49.8 | 0.0 |
| $\omega(2,1,4,7)$ | 0.0 | −35.6 | 0.0 |
| | Transition State | | |
| $R(1,2)$ | 1.519 | 1.587 | 1.530 |
| $R(2,5)$ | 1.302 | 1.330 | 1.328 |
| $R(1,4)$ | 1.330 | 1.364 | 1.345 |
| $R(5,7)$ | 1.167 | 1.248 | 1.236 |
| $R(4,7)$ | 1.444 | 1.492 | 1.469 |
| $\theta(1,2,5)$ | 111.2 | 110.1 | 113.5 |
| $\theta(4,1,2)$ | 106.4 | 106.1 | 107.4 |
| $\theta(2,5,7)$ | 98.4 | 100.2 | 94.8 |
| $\theta(4,7,5)$ | 129.5 | 126.0 | 131.0 |
| $\theta(1,4,7)$ | 94.5 | 95.8 | 93.3 |
| $\omega(5,2,1,3)$ | −179.5 | −166.8 | 180.0 |
| $\omega(6,2,1,4)$ | −179.2 | −165.5 | 180.0 |
| $\omega(5,2,1,4)$ | 0.6 | 14.6 | 0.0 |
| $\omega(2,1,4,7)$ | −0.5 | −11.6 | 0.0 |

[a] Lengths are in angstroms and angles in degrees.

longer. The $C_1-C_2$ bond lengths $R(1,2)$ at the AM1 and MP2 levels are 1.55 and 1.51 Å, respectively. The $\omega(5,2,1,3)$ value, which is a dihedral angle for $N_5-C_2-C_1-N_3$, is very dependent on the level of calculation. The $\omega(5,2,1,3)$ values for oxalamidine from the AM1 and MP2 methods are −122.4° and −166.8°, respectively. The optimized structure of the intermediate at the MP2 level is planar and has $C_{2v}$ symmetry with an axis along the $C_1-C_2$ bond. The H-bond distance between $N_4$ and $H_7$, $R(4,7)$, is 2.08 Å. The intermediate optimized at the AM1 level has $C_2$ symmetry, and the $R(4,7)$ value is 2.56 Å. The H-bond distance is 0.48 Å larger than the MP2 value. The atoms $N_6$, $C_2$, and $N_5$ define a plane, and the atoms $N_3$, $C_1$, and $N_4$ define another plane. The angle between these two planes is 49.8°. The TS structure optimized at the MP2 level is almost planar, but that at the AM1 level is twisted. The $R(4,7)$ and $R(5,7)$ values at the MP2 level are 1.45 and 1.17 Å, respectively, and those at the AM1 level are 1.49 and 1.25 Å, respectively. The AM1 level of theory tends to generate a loose transition state. The $R(1,2)$ value at the MP2 level is 0.07 Å shorter than the

**Table 3.** Specific Reaction Parameters[a]

| atom | param | AM1-SRP | AM1 |
|---|---|---|---|
| H | $\zeta_S$ | 1.048078 | 1.188078 |
| H | $\alpha$ | 3.252324 | 2.882324 |
| N | $G_{SP}$ | 11.36 | 12.66 |
| N | $\beta_S$ | −21.199110 | −20.299110 |
| N | $\beta_P$ | −17.338666 | −18.238666 |
| N | $\alpha$ | 2.987286 | 2.947286 |
| C | $G_{P2}$ | 9.34 | 9.84 |
| C | $\zeta_P$ | 1.485116 | 1.685116 |
| C | $\beta_S$ | −10.815783 | −15.715783 |
| C | $\beta_P$ | −12.719283 | −7.719283 |

[a] $\zeta_S$ = Slater exponent of the s-orbital. $\zeta_P$ = Slater exponent of the p-orbital. $\alpha$ = core−core repulsion intergral. $G_{SP}$ = one-center electron repulsion integral, $G_{SP}$ = (ss|pp). $G_{P2}$ = one-center electron repulsion integral, $G_{P2}$ = (ss|p′p′). $\beta_S$ = s-orbital bond parameter used in calculating the resonance integral. $\beta_P$ = p-orbital bond parameter used in calculating the resonance integral.

corresponding AM1 value. The geometries for oxalamidine, the intermediate, and the TS from the AM1 calculations are quite different from those of high-level ab initio calculations.

The NDDO level of semiempirical MO calculation with standard AM1 parameters gives 35.72 and 52.07 kcal mol$^{-1}$ for $\Delta E$ and $\Delta E^*$, respectively. These $\Delta E$ and $\Delta E^*$ values are much higher than the corresponding G2* values. Since the AM1 level of theory does not correctly represent the energetics for the double proton transfer and geometries for R, I, and TS, the AM1 parameters should be adjusted before they are used in the direct semiempirical dynamics calculation. We have modified the standard AM1 parameters, first, to reproduce the structures of R, I, and TS and, second, to reproduce energetics at the G2* level and the frequencies from the MP2 level of calculation. We initially changed 32 parameters by hand (13 parameters each for C and N, and 6 for H) and monitored the variation of energies and structures in terms of each parameter. Parameters, which change the energies and structures, were selected to reproduce the high-level ab initio calculation. Ten parameters were chosen and adjusted as listed in Table 3. The adjusted parameters are called specific reaction parameters (AM1-SRP). The $\Delta E$ and $\Delta E^*$ values from the AM1-SRP calculations are 20.71 and 25.05 kcal mol$^{-1}$, respectively. These agree almost perfectly with those from the G2* level of calculation. The frequencies for R, I, and TS from the MP2 and AM1-SRP methods are listed in Table 4. The AM1-SRP frequencies show fairly good agreement with those from the MP2(full)/6-31G(d,p) calculation. The reaction coordinate frequency is 1284i cm$^{-1}$, which is about 200 cm$^{-1}$ larger than the MP2 frequency, but much smaller than the AM1 and HF frequencies. The geometric parameters for optimized structures of R, I, and TS from the AM1-SRP method are also listed in Table 2. They agree very well with those from the MP2(full)/6-31G(d,p) method. For oxalamidine, the $R$(5,7) and $\omega$(5,2,1,3) values at the AM1-SRP level are 2.296 Å and −172.4°, respectively, which agree very well with the MP2 results. The structure of the intermediate at the AM1 level is twisted, but planar at the AM1-SRP level. The $R$(5,7) value is 2.104 Å, which is very close to the MP2 value. The TS structure is almost planar at the MP2 level but twisted at the AM1 level. The AM1-SRP calculation also predicts a planar TS, which agrees with the MP2 results.

Figure 2 shows the Born−Oppenheimer potential energy and the adiabatic ground-state potential energy along the MEP for the first proton transfer from reactant to intermediate calculated from the AM1-SRP method. The adiabatic ground-state potential energy, $V_a^G$, is the sum of the Born−Oppenheimer potential

**Table 4.** Calculated Frequencies for Oxalamidine (R), the Intermediate (I), and the Transition State (TS)[a]

| R | | I | | TS | |
|---|---|---|---|---|---|
| MP2 | AM1-SRP | MP2 | AM1-SRP | MP2 | AM1-SRP |
| 3597 | 3462 | 3593 | 3459 | 3616 | 3502 |
| 3596 | 3456 | 3593 | 3450 | 3543 | 3487 |
| 3449 | 3438 | 3406 | 3444 | 3498 | 3444 |
| 3446 | 3437 | 3405 | 3439 | 3399 | 3440 |
| 3372 | 3332 | 3277 | 3080 | 3391 | 3248 |
| 3371 | 3327 | 3247 | 3056 | 2115 | 2031 |
| 1682 | 1991 | 1722 | 1989 | 1739 | 1965 |
| 1643 | 1974 | 1649 | 1877 | 1669 | 1831 |
| 1572 | 1669 | 1549 | 1716 | 1538 | 1670 |
| 1569 | 1560 | 1434 | 1543 | 1435 | 1538 |
| 1461 | 1436 | 1421 | 1373 | 1348 | 1415 |
| 1321 | 1421 | 1322 | 1353 | 1178 | 1159 |
| 1116 | 1132 | 1133 | 1142 | 1116 | 1120 |
| 1113 | 1085 | 1108 | 1107 | 1101 | 1063 |
| 1080 | 1012 | 1057 | 1033 | 1073 | 1036 |
| 1066 | 986 | 1020 | 990 | 1039 | 1014 |
| 838 | 923 | 826 | 921 | 771 | 920 |
| 827 | 803 | 764 | 891 | 764 | 806 |
| 760 | 782 | 756 | 800 | 758 | 759 |
| 713 | 727 | 740 | 787 | 708 | 680 |
| 587 | 650 | 689 | 594 | 689 | 651 |
| 573 | 640 | 621 | 575 | 586 | 598 |
| 528 | 568 | 550 | 573 | 568 | 593 |
| 523 | 552 | 531 | 546 | 534 | 541 |
| 460 | 473 | 476 | 529 | 466 | 503 |
| 420 | 457 | 392 | 515 | 393 | 470 |
| 410 | 419 | 368 | 429 | 329 | 398 |
| 355 | 380 | 364 | 404 | 308 | 370 |
| 315 | 353 | 291 | 272 | 83 | 109 |
| 100 | 17 | 86 | 62 | 1026i | 1284i |

[a] The MP2 frequencies were weighted by 0.95.

($V_{MEP}$) and the local zero-point energies. The reaction coordinate for the first proton transfer from oxalamidine to intermediate is very endoergic. The second proton transfer is just the reverse of the first. Since two protons are transferred, there are four possible reactions depending on the isotopic substitution as depicted in R1−R4. Rate constants with and without tunneling

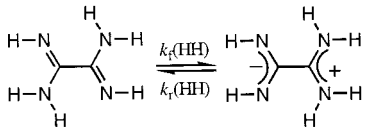


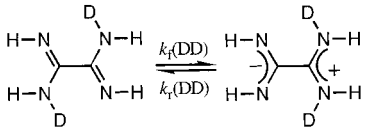


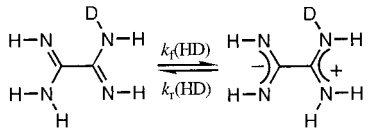


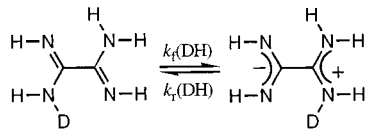


were also calculated in the temperature range 250−450 K, and they are listed in Table 5 for reactions R1, R2, R3, and R4. The transmission coefficients using the SCT, LCT, and $\mu$OMT approximations are denoted as $\kappa^{SCT}$, $\kappa^{LCT}$, and $\kappa^{\mu OMT}$, respec-

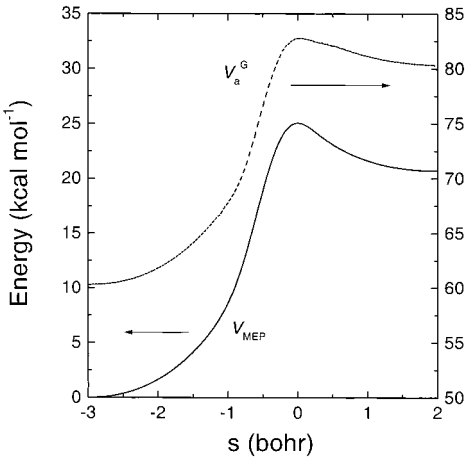


**Figure 2.** Potential and adiabatic energies along the minimum energy path.

**Table 5.** Transmission Coefficients and Rate Constants for R1, R2, R3, and R4

| T (K) | $\kappa^{SCT}$ | $\kappa^{LCT}$ | $\kappa^{\mu OMT}$ | $k_f$ | $k_r$ | $k_f^{\mu OMT}$ | $k_r^{\mu OMT}$ |
|---|---|---|---|---|---|---|---|
| | | | | R1 | | | |
| 250 | 3.60 | 3.28 | 3.63 | 4.49E−08 | 4.26E+10 | 1.63E−07 | 1.55E+11 |
| 300 | 2.49 | 2.32 | 2.51 | 8.04E−05 | 9.55E+10 | 2.02E−04 | 2.40E+11 |
| 350 | 1.97 | 1.87 | 1.99 | 1.71E−02 | 1.72E+11 | 3.40E−02 | 3.42E+11 |
| 400 | 1.69 | 1.62 | 1.70 | 9.55E−01 | 2.69E+11 | 1.63E+00 | 4.58E+11 |
| 450 | 1.52 | 1.47 | 1.53 | 2.20E+01 | 3.83E+11 | 3.36E+01 | 5.85E+11 |
| | | | | R2 | | | |
| 250 | 3.21 | 2.76 | 3.21 | 8.01E−09 | 1.06E+10 | 2.57E−08 | 3.41E+10 |
| 300 | 2.24 | 2.01 | 2.24 | 1.85E−05 | 2.92E+10 | 4.14E−05 | 6.53E+10 |
| 350 | 1.80 | 1.66 | 1.80 | 4.70E−03 | 6.07E+10 | 8.47E−03 | 1.09E+11 |
| 400 | 1.57 | 1.47 | 1.57 | 3.01E−01 | 1.06E+11 | 4.71E−01 | 1.66E+11 |
| 450 | 1.43 | 1.36 | 1.43 | 7.68E+00 | 1.63E+11 | 1.09E+01 | 2.33E+11 |
| | | | | R3 | | | |
| 250 | 3.46 | 3.23 | 3.51 | 4.30E−08 | 4.81E+10 | 1.51E−07 | 1.69E+11 |
| 300 | 2.42 | 2.30 | 2.45 | 7.75E−05 | 1.06E+11 | 1.90E−04 | 2.59E+11 |
| 350 | 1.93 | 1.86 | 1.96 | 1.65E−02 | 1.87E+11 | 3.23E−02 | 3.67E+11 |
| 400 | 1.67 | 1.62 | 1.68 | 9.27E−01 | 2.90E+11 | 1.56E+00 | 4.88E+11 |
| 450 | 1.50 | 1.47 | 1.52 | 2.14E+01 | 4.10E+11 | 3.24E+01 | 6.21E+11 |
| | | | | R4 | | | |
| 250 | 3.17 | 2.78 | 3.17 | 8.38E−09 | 9.41E+09 | 2.66E−08 | 2.99E+10 |
| 300 | 2.21 | 2.02 | 2.21 | 1.92E−05 | 2.64E+10 | 4.26E−05 | 5.84E+10 |
| 350 | 1.79 | 1.67 | 1.79 | 4.87E−03 | 5.56E+10 | 8.70E−03 | 9.93E+10 |
| 400 | 1.56 | 1.48 | 1.56 | 3.11E−01 | 9.78E+10 | 4.83E−01 | 1.52E+11 |
| 450 | 1.42 | 1.36 | 1.42 | 7.91E+00 | 1.53E+11 | 1.12E+01 | 2.16E+11 |

tively. The transmission coefficients are not very large. They are reasonable compared to the tunneling coefficient estimated in typical single-proton-transfer reactions.[2,3,65] The $\kappa^{LCT}$ values are smaller than $\kappa^{SCT}$ at all temperatures. The $\kappa^{\mu OMT}$ values are approximately the same as $\kappa^{SCT}$ values. These results suggest that the reaction path curvature is not large, although this reaction has the heavy−light−heavy mass combination. The first step of this reaction is very endothermic, and the TS resembles the intermediate. The location of the transferring proton at the TS is close to its location in the intermediate. Generally, the reaction path curvature is small when the TS is very late or early, so the SCT method would be appropriate to calculate the tunneling probability. When tunneling is very important, the representative tunneling path (RTP), where the thermally weighted transmission probability has a maximum, is further from the top of the barrier. When tunneling is not very important, it is closer to the top. The RTP from the SCT method goes from $s = -0.16$ to $s = 0.48$ at 300 K. The adiabatic energy at the pretunneling configuration of RTP is 82.10 kcal mol$^{-1}$, which is 0.67 kcal mol$^{-1}$ below the top of the adiabatic energy barrier. The potential energy at the pretunneling configuration is 24.46 kcal mol$^{-1}$, which is only 0.60 kcal mol$^{-1}$ below the top of the potential energy barrier. However, the potential energy at the posttunneling configuration is 23.19 kcal mol$^{-1}$, which is 1.86 kcal mol$^{-1}$ below the top. This indicates that the zero-point energy at the posttunneling configuration is larger that at the pretunneling configuration.

(65) Kim, Y.; Truhlar, D. G.; Kreevoy, M. M. *J. Am. Chem. Soc.* **1991**, *113*, 7837.

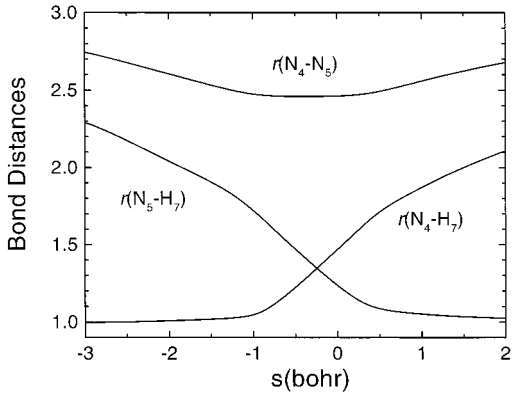


**Figure 3.** Bond distances along the minimum energy path. Bond distances are in angstroms.

Figure 3 shows the $N_4-H_7$ and $N_5-H_7$ bond lengths, and the distance between $N_4$ and $N_5$ atoms along the minimum energy path. From reactant ($s = -\infty$) to $s = -1.0$, the $N_4-H_7$ bond length is hardly changed, but the distance between $N_4$ and $N_5$ is changed from 2.75 to 2.48 Å. The closest distance between $N_4$ and $N_5$ is 2.46 Å at $s = -0.4$; therefore, about 95% of its change occurs before $s = -1.0$. The bond lengths for $N_4-H_7$ and $N_5-H_7$ are changed from 1.00 to 1.05 Å and from 2.29 to 1.72 Å, respectively, between $s = -\infty$ and $s = -1.0$. Between $s = -1.0$ and $s = 0.5$, the $N_4-N_5$ distance is hardly changed, but the $N_4-H_7$ and $N_5-H_7$ bond lengths are changed from 1.05 to 1.71 Å and from 1.72 to 1.09 Å, respectively. It is mostly heavy atoms that move when the reaction goes from reactant to $s = -1.0$. After this point a proton moves rapidly without changing the distance between heavy atoms very much. This suggests that the hydrogenic motion is well separated from the heavy atom motion along the reaction coordinate. This phenomenon has been observed before in concerted double proton transfers. Shida et al. have reported a reaction path Hamiltonian calculation for the double proton transfer in formic acid dimer and shown that the tunneling path is very different from the MEP.[17] While a proton hops by tunneling, heavy atoms do not move much. Before the tunneling occurs, heavy atoms move mostly to bring two reactants close together, while the hydrogenic motion is minimal. These phenomena have also been observed from the direct semiempirical dynamics calculations for the double proton transfer in formic acid dimer[20] and in monohydrated formamidine.[22]

The bond lengths for $N_4-H_7$ at the pre- and posttunneling configurations are 1.39 and 1.70 Å, respectively, and those for $N_5-H_7$ are 1.31 and 1.09 Å, respectively. The distances between the two nitrogen atoms at the pre- and posttunneling configurations are 2.46 and 2.49 Å, respectively. The proton hops about 0.32 Å by tunneling, but heavy atoms move only 0.03 Å while tunneling occurs. Truhlar and co-workers have reported direct dynamics calculations for the hydrogen atom transfer in the [1,5]-sigmatropic rearrangement of *cis*-1,3-pentadiene, where the hydrogen atom moves about 0.2 Å by tunneling between two carbons at 470 K.[43] They have also studied the hydrogen-transfer reaction between $CF_3$ and $CD_3H$, where the hydrogen

**Table 6.** Overall Rate Constants for the Double Proton Transfer, the Double Deuterium Transfer, and the Proton and Deuterium Transfer with and without Tunneling Contribution

| $T$ (K) | $k_o$(HH) | $k_o^{\mu OMT}$(HH) | $k_o$(DD) | $k_o^{\mu OMT}$(DD) | $k_o$(HD) | $k_o^{\mu OMT}$(HD) |
|---|---|---|---|---|---|---|
| 200 | 3.01E−13 | 2.07E−12 | 3.65E−14 | 2.29E−13 | 6.82E−14 | 4.26E−13 |
| 250 | 2.24E−08 | 8.15E−08 | 4.00E−09 | 1.29E−08 | 7.05E−09 | 2.27E−08 |
| 300 | 4.02E−05 | 1.01E−04 | 9.24E−06 | 2.07E−05 | 1.55E−05 | 3.49E−05 |
| 350 | 8.54E−03 | 1.70E−02 | 2.35E−03 | 4.23E−03 | 3.78E−03 | 6.88E−03 |
| 400 | 4.78E−01 | 8.14E−01 | 1.50E−01 | 2.36E−01 | 2.34E−01 | 3.71E−01 |
| 450 | 1.10E+01 | 1.68E+01 | 3.84E+00 | 5.47E+00 | 5.80E+00 | 8.36E+00 |
| 500 | 1.35E+02 | 1.91E+02 | 5.15E+01 | 6.86E+01 | 7.59E+01 | 1.02E+02 |

atom moves about 0.39 Å by tunneling but the C−C distance changes only 0.08 Å at 367.8 K.[44] In the direct semiempirical dynamics calculations for the concerted double proton transfers in formic acid dimer[20] and in monohydrated formamidine,[22] two protons move about 0.43 and 0.62 Å by tunneling at 300 K, respectively. The distance that a proton jumps by tunneling in oxalamidine is smaller than the distances in the concerted double proton transfers. However, it is larger than those for a general single proton or hydride transfer in solution, although the transmission coefficient at 300 K is quite close to the typical values observed in many single proton transfer reactions. Consider for example the potential energy surfaces for single hydride transfer between $NAD^+$ analogues in solution. Analytical potential energy functions were fitted to reproduce experimental kinetic isotope effects for the hydride transfer reactions.[65] The RTP occurs about 1 kcal mol$^{-1}$ below the top of the potential energy barrier, and the tunneling distance at the RTP for the hydride transfer between $NAD^+$ analogues is about 0.1 Å.

Overall rate constants for the stepwise reactions were calculated by using the steady-state approximation as shown in R5 with eq 5. The forward and reverse rate constants with and

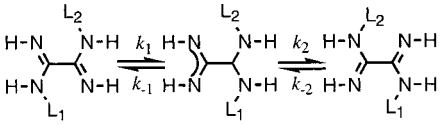


(R5)

$L_1 = L_2 = H$ or D

$$k_o = k_1 k_2 / (k_{-1} + k_2) \quad (5)$$

without tunneling correction listed in Table 5 were used to calculate overall rate constants. The results are listed in Table 6. The overall rate constants for the proton−proton, deuterium−deuterium, and proton−deuterium transfer reactions were denoted as $k_o$(HH), $k_o$(DD), and $k_o$(HD), respectively. The Arrhenius plots for the $k_o$ values are linear as shown in Figure 4, and the activation energy and the preexponential factor for the HH transfer are 21.3 kcal mol$^{-1}$ and $3.54 \times 10^{11}$, respectively. Limbach et al. have determined the rate constants and KIEs for the double proton transfer in bicyclic oxalamidines using the dynamic NMR method in acetonitrile and methylcyclohexane.[40,41] They found that the Arrhenius activation energy for the HH transfer is about 13.8 kcal mol$^{-1}$, which is smaller than the value in this study. Some of the experimental data are included in Figure 4, and their Arrhenius plots are linear within the temperature range measured. The Arrhenius preexponential factor agrees well with the experimental value. Limbach et al. have calculated geometries and barrier heights for proton transfer in various oxalamidines using a semiempirical quantum mechanical method.[42] They have reported that the barrier height depends mostly on the strength of the hydrogen bond and the stabilization of the charges created by the substituents such as phenyl or methylene groups. In the bicyclic oxalamidine connected by a five-membered ring, the N−N distance was

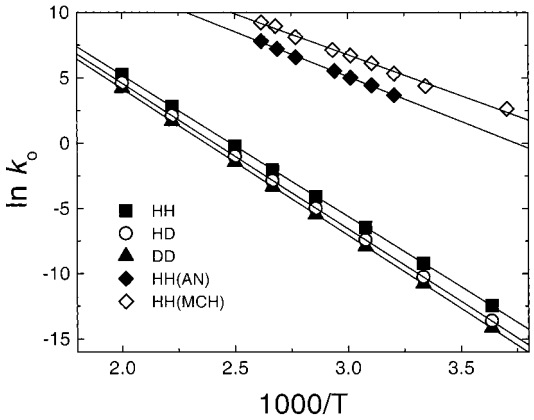


**Figure 4.** Arrhenius plot for the calculated overall rate constants using the $\mu$OMT method, and for the experimental values measured in acetonitrile (AN) and methylcyclohexane (MCH).

longer than that in the oxalamidine, which makes the hydrogen bond weaker. The barrier height was much larger than that of oxalamidine, which was attributed to the ring strain.[42] In bicyclic oxalamidines used in the NMR experiments, two nitrogen atoms, $N_3$ and $N_4$, are connected by a seven-membered ring, which would make it more flexible. The $N_3-C_1-N_5$ angle becomes larger, and the distance between $N_4$ and $N_5$ becomes smaller. The atoms $N_4$ and $N_5$ are hydrogen bond donor and acceptor, and reducing the distance between them makes the hydrogen bond stronger. The strong hydrogen bond in a flexible ring system would lower the potential energy barrier.

The calculated KIEs using overall rate constants at the various temperatures are listed in Table 7. The KIEs for HH/DD, HH/HD, and HD/DD were calculated by $k_o^{\mu OMT}$(HH)/$k_o^{\mu OMT}$(DD), $k_o^{\mu OMT}$(HH)/$k_o^{\mu OMT}$(HD), and $k_o^{\mu OMT}$(HD)/$k_o^{\mu OMT}$(DD), and they are 4.88, 2.89, and 1.69, respectively, at 300 K, which agree very well with the experimental values measured in methylcyclohexane (MCH).[40] The tunneling contributions to the KIEs for HH/DD, HH/HD, and HD/DD are 1.12, 1.11, and 1.01, respectively, at 300 K. They are small compared with those for concerted double proton transfers,[20,22] but reasonable for typical single proton transfer.[2,3] The rate constants and KIEs have also been measured in acetonitrile (AN). The rate constants in AN are larger than those in MCH as depicted in Figure 4, and the KIEs are also larger. In general, when the barrier is lowered, it becomes wider. Then the tunneling effect is reduced to give smaller KIEs. The experimental KIEs for HH/DD, HH/HD, and HD/DD at 298 K are 5.2, 3.2, and 1.6, respectively. We have calculated the solvent effect on the energetics and reaction coordinate frequency at the B3LYP/6-31+G(d,p) level using the Onsager dielectric continuum model.[64] The results are listed in Table 1. The solvent effect reduced both $\Delta E$ and $\Delta E^*$ values, but the $\Delta E$ value was reduced further, which provides more space on the potential energy surface that a proton can tunnel through. The reaction coordinate frequency was also increased,

**Table 7.** Kinetic Isotope Effects at Various Temperatures

| T (K) | $k_o$(HH)/$k_o$(DD) | $k_o^{\mu OMT}$(HH)/$k_o^{\mu OMT}$(DD) | $k_o$(HH)/$k_o$(DD) | $k_o^{\mu OMT}$(HH)/$k_o^{\mu OMT}$(HD) | $k_o$(HD)/$k_o$(DD) | $k_o^{\mu OMT}$(HD)/$k_o^{\mu OMT}$(DD) |
|---|---|---|---|---|---|---|
| 200 | 8.25 | 9.06 | 4.41 | 4.87 | 1.87 | 1.86 |
| 250 | 5.60 | 6.33 | 3.18 | 3.59 | 1.76 | 1.77 |
| 300 | 4.35 | 4.88 | 2.60 | 2.89 | 1.68 | 1.69 |
| 350 | 3.64 | 4.01 | 2.26 | 2.47 | 1.61 | 1.63 |
| 400 | 3.18 | 3.45 | 2.04 | 2.20 | 1.55 | 1.57 |
| 450 | 2.86 | 3.07 | 1.89 | 2.01 | 1.51 | 1.53 |
| 500 | 2.63 | 2.79 | 1.78 | 1.87 | 1.47 | 1.49 |

**Table 8.** Equilibrium Isotope Effects (EIEs) and $\gamma$-Deuterium Secondary KIEs for the First Proton Transfer with and without Tunneling

| T (K) | s-KIE$_{qc}$ | s-KIE$^{\mu OMT}$ | EIE | *T* (K) | s-KIE$_{qc}$ | s-KIE$^{\mu OMT}$ | EIE |
|---|---|---|---|---|---|---|---|
| 200 | 1.051 | 1.110 | 1.219 | 400 | 1.031 | 1.043 | 1.113 |
| 250 | 1.043 | 1.080 | 1.176 | 450 | 1.028 | 1.038 | 1.101 |
| 300 | 1.038 | 1.062 | 1.148 | 500 | 1.025 | 1.033 | 1.090 |
| 350 | 1.034 | 1.051 | 1.128 | | | | |

so the tunneling effect will be increased in a polar solvent to give larger KIEs.

The secondary KIE has long been used to estimate the position of the TS along the reaction coordinate.[2,3] The $\gamma$-deuterium secondary KIEs were given by the ratio of the rate constants for R1 to R3, which are listed in Table 8 along with the equilibrium isotope effects (EIEs). The EIE and quasiclassical $\gamma$-deuterium secondary KIE at 300 K are 1.148 and 1.038, respectively. This indicates that isotopically sensitive force constants at the TS are changed about 26% with respect to those at the intermediate by the isotopic substitution at the $\gamma$-position. Although the geometric parameters for TS are closer to those of the intermediate (TS is late geometrically), the force constants are still closer to those of the reactant (TS is early in terms of force constants). These results indicate that proton transfer and the change in the force constants are asynchronous.

We have also calculated the rate constants and equilibrium constants with isotopic substitution at the $\alpha$-position. The $H_{12}$ atom was replaced with a deuterium. The calculated rate constant without tunneling and the equilibrium constant are $8.22 \times 10^{-5}$ and $8.96 \times 10^{-16}$, respectively, at 300 K. The EIE and quasiclassical $\alpha$-deuterium secondary KIE were calculated from these values, which yield 0.939 and 0.978, respectively. The EIE and quasiclassical secondary KIE are inverse in this reaction. The force constants at the $\alpha$-position of the TS are changed about 36% with respect to those at the intermediate. It is interesting that the force constants of the $\alpha$-proton are changed more than those of the $\gamma$-proton. These result suggest that the closer the isotopic substitution to the reaction center the larger the change in the force constants at the TS. In other words, the force constants of secondary protons closer to the reaction center are correlated more with the location of the TS than those far from the reaction center.

## Concluding Remarks

The double proton transfer in oxalamidine has been studied by direct semiempirical dynamics calculations using variational transition state theory with multidimensional semiclassical tunneling approximations. Two protons are transferred stepwise with an intermediate, which has $C_{2v}$ symmetry. The hydrogenic motion is well separated from the heavy atom motion along the MEP. The tunneling correction at 300 K is about 2.51. This value is reasonable compared to results for the single proton transfer. The calculated KIEs for HH/DD, HH/HD, and HD/DD are 4.88, 2.89, and 1.69, respectively, which agree very well with the experimental values. The representative tunneling path (RTP) at 300 K occurs about 0.67 kcal mol$^{-1}$ below the top of the adiabatic energy barrier. The distance that a proton hops by tunneling is 0.32 Å, which is larger than the tunneling distance in typical single proton transfers in solution. Quasiclassical secondary KIEs reveal that the nuclear motion (proton transfer) and the change in the force constants are asynchronous. That is, the structure of the TS cannot be deduced from the secondary isotope effects.

**Acknowledgment.** We acknowledge financial support from the SERI Supercomputer Center through the 1998 CRAY R&D Grant Program. We thank Professor Maurice M. Kreevoy, Department of Chemistry, University of Minnesota, for helpful comments.

JA984242Z